Dynamics and lateral interactions of dipolar chains

Eric M. Furst* and Alice P. Gast†
Department of Chemical Engineering, Stanford University, Stanford, California 94305-5025
(Received 25 June 2000)

The dynamics and lateral interactions of dipolar chains in magnetorheological suspensions determine the long-time microscopic structure and resulting rheological response. In this paper we characterize proposed lateral interaction mechanisms and their implications for long-time coarsening of structure and compare them to direct measurements of the lateral interaction of dipolar chains using optical trap micromanipulation. We observe a long-range far-field attraction between flexible chains, while the near-field interaction can be repulsive or attractive. At high field strengths, we observe the short-range attraction of rigid chains. Chain dynamics measured with videomicroscopy and diffusing wave spectroscopy are described by a local-mode model and are consistent with fluctuation-mediated interaction theories. The subdiffusive behavior at intermediate and long times scales as $t^{0.75}$, identical to semiflexible molecules. Finally, we show examples of how defects in chains can create lateral attractions or repulsions.

PACS number(s): 82.70.Dd, 83.10.Pp, 83.20.Hn

I. INTRODUCTION

Magnetorheological (MR) suspensions consist of superparamagnetic particles dispersed in a nonmagnetic fluid. Like all colloidal systems, the rheological properties of MR suspensions are intimately tied to the microscopic structure and interparticle forces [1]. During the application of an external magnetic field to a MR suspension, the particles acquire dipole moments proportional to the field strength. When the field-induced interaction between particles is in sufficient excess of the thermal energy kT, the particles rapidly aggregate into chains of dipoles aligned in the field direction. This microstructural transition is responsible for a dramatic rheological transition, demonstrated by the sudden onset of a large yield stress. The tunability, speed, and magnitude of the rheological response make MR suspensions attractive for interfacing mechanical systems to electronic controls. Several commercial passive and semiactive applications already exist, with more expected in the future, including the possible use of MR suspension dampers to control a building's response to seismic events [2,3]

In this paper we focus on the dynamics and mechanisms determining the behavior of MR suspensions beyond the initial formation of individual dipolar chains. For instance, it has been observed that once long chains form they laterally coalesce to create columns or networks in more concentrated suspensions [4,5]. Therefore, the physical description of chain coalescence responsible for lateral aggregation is essential for understanding the structural evolution in MR systems, especially as the volume fraction increases.

The surprising fact that chains of dipolar particles can attract one another at long range to form aggregates has led to the development of several models [6–9]. The first theory to predict long-range interaction of dipolar chains is due to Halsey and Toor (HT) [6,7], who noted that the coupling of strong Landau-Peierls thermal fluctuations of chains induces a Keesom-like interaction between them. More recent models expand the HT theory to take into account the time scales of interaction [8,9], and a recent work by Martin and coworkers considers the effects of topological defects in chains to show that the resulting perturbations in the local lateral field can drive coarsening in the absence of thermal fluctuations [10].

It still, however, remains to understand the microscopic lateral interaction in detail. Experimental observations are limited, and usually infer suspension structure and underlying interactions from videomicroscopy, static light scattering, and optical transmittance [4,9–12]. In this paper, we utilize our ability to manipulate dipolar chains with optical traps to measure the lateral interactions directly. We will begin in Sec. II with an overview of several theories of the lateral interaction of dipolar chains, including the interaction of rigid chains and the effects of thermal fluctuations and chain defects. We focus on the regimes of applicability for the various lateral interaction theories, illustrating that each mechanism applies to a distinct range of suspension concentration and field strength.

In Sec. III we present the experimental techniques used to study lateral chain interactions, including our use of optical trapping and videomicroscopy. We characterize the dynamics of dipolar chains over a range of interaction strengths to determine whether or not the actual dynamics of dipolar chains are consistent with the theories of fluctuation-based interactions. Using optical trapping, we apply micromanipulation and dynametric capabilities to *directly* measure lateral chain interactions in the far and near fields, and observe the effects of chain rigidity and finite length. The results of our experiments are discussed in Sec. IV. Finally, we summarize this work in Sec. V.

II. LATERAL INTERACTIONS AND STRUCTURAL COARSENING

A. Rigid chain interaction

Chains of rigid dipoles are expected to exhibit short-range interactions. We follow the derivation of Halsey and Toor

*Present address: Institut Curie, Laboratoire de Physico-Chimie, 11 rue Pierre et Marie Curie, 75005 Paris, France.
†Author to whom all correspondence should be addressed. Electronic address: alice@chemeng.stanford.edu

who solved the electrostatic problem to calculate the lateral field around an infinite chain of dipoles, showing that it decays exponentially with distance ρ in the plane orthogonal to the chain. Simply extending this solution to the magnetic case yields

$$H(\rho,z)\approx-(2\pi)^2\left(\frac{m}{4\pi\mu_0\rho^2 a}\right)\left(\frac{a}{\rho}\right)^{1/2}e^{-2\pi\rho/a}\cos(2\pi z/a), \tag{1}$$

where z is the position along the chain in the applied field direction, m is the particle moment, and μ_0 is the vacuum permeability. In Eq. (1), the lateral field surrounding the chain gives rise to either a repulsive or an attractive interaction depending on whether the particles in neighboring chains are in or out of registry. The lateral interaction between two chains is an integral over the dipole moment density with the field,

$$U(\rho)=\frac{2}{4\pi\mu_0 L}\int_0^L dz\left[m\sum_n\ \delta(z-2na)\right]H(\rho,z)$$

$$=\pm(2\pi)^2\frac{2m^2}{4\pi\mu_0\rho^2 a}\left(\frac{a}{\rho}\right)^{1/2}e^{-2\pi\rho/a}, \tag{2}$$

noting that the particle positions are denoted as points separated by a lattice spacing of $2na$ using the Dirac delta function $\delta(z)$.

The lateral interactions in electrorheological (ER) suspensions, the electrical analog to MR systems, can in general be treated as infinite chains of dipoles due to image charges induced in the conducting electrodes. In the MR suspensions, this is typically not the case, since the boundary is often a low-permeability material. Consequently, magnetic chains may have significant interaction between the free dipoles at each of the ends. We illustrate this by calculating the interaction of rigid dipolar chains of finite length.

The details of our calculations are described in [13]. Briefly, we account for mutual induction between particles and self-consistently solve the magnetic moments and interactions between particles for arbitrary arrangements by numerical iteration. The magnetic moment of each particle i is

$$\mathbf{m}_i=\frac{4}{3}\pi a^3\mu_0\chi\left[\mathbf{H}_0+\sum_{j\neq i}\frac{3\hat{\mathbf{r}}(\hat{\mathbf{r}}\cdot\mathbf{m}_j)-\mathbf{m}_j}{4\pi\mu_0 r^3}\right], \tag{3}$$

where the summation takes into account the induced field from all other particles. Pairs of particles interact via an anisotropic dipolar potential

$$U_{ij}^{dip}=\frac{1}{4\pi\mu_0}\frac{\mathbf{m}_i\cdot\mathbf{m}_j-3(\hat{\mathbf{r}}\cdot\mathbf{m}_i)(\hat{\mathbf{r}}\cdot\mathbf{m}_j)}{r^3}. \tag{4}$$

$\mathbf{r}$ is the vector between particle centers and $\hat{\mathbf{r}}$ is the unit vector $\mathbf{r}/r$.

To calculate the interaction, two chains of 50 particles are aligned parallel to one another along the field axis z and the total energy $U_{tot}=\Sigma_i\Sigma_{j>i}U_{ij}^{dip}$ determined as a function of lateral separation ρ. In Fig. 1 we illustrate several cases of chain interaction. For aligned chains, the interaction changes from the far field to the near field. For $\rho>2d$ the energy is repulsive because the chain ends dominate the interaction. At distances $\rho<2d$, the interaction is strong and either repulsive or attractive depending on whether the particles in neighboring chains are in or out of registry, similar to the behavior of infinite chains discussed above. In Fig. 1 we also show that the interaction of chain ends can be minimized by offsetting the chains along the z axis, in this case by half the chain length, $N/2$. This eliminates the far-field interaction, leaving only a near-field attraction or repulsion depending on the registry of the particles. Note that U_{tot} scales with λ in all cases.

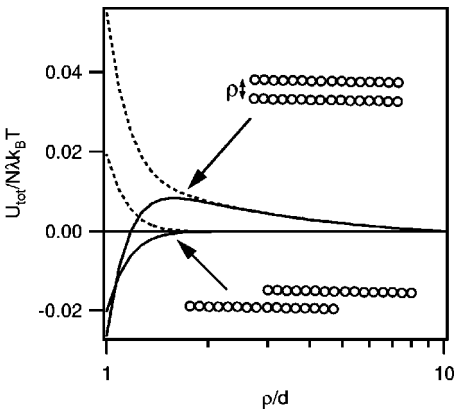

FIG. 1. The calculated interaction between rigid dipolar chains. Dashed and solid lines indicate that particles in the neighboring chain are in registry or out of registry by $d/2$, respectively. A far-field repulsion is observed for chains with aligned ends. Chains offset by $N/2$ exhibit only the short-range attraction.

Equation (2) shows that the interaction between two dipolar chains is the integral of the lateral field with the dipole moment density. For the case of rigid chains, the particles occupy discrete lattice spacings. In a real system, however, we expect thermal fluctuations of chains and defects to cause variations in the dipole moment density and thus the lateral interaction chains experience. These considerations were first addressed by Halsey and Toor [6], and will be discussed below.

B. Halsey-Toor model

As one-dimensional structures suspended in a three-dimensional fluid, dipolar chains exhibit strong Landau-Peierls fluctuations [14]. Halsey and Toor show that these fluctuations result in long-range coupling between dipolar chains, which results in an attractive interaction with a power-law decay [6]. This is not entirely surprising, since fluctuation-induced interactions are common in colloid science. Examples of interactions generated through thermal and quantum fluctuations include the London and Keesom interactions [15]. Here we briefly consider the HT model and identify its principal results.

According to the HT model, longitudinal and transverse particle fluctuations of wave vector $\mathbf{k}$ in a dipolar chain create local variations in the concentration of dipoles. This in turn introduces fluctuations in the lateral field. The total interaction energy of two chains is the sum of the interaction energy between their fluctuations and the energy of deforma-

tion required for the fluctuation mode.

Halsey and Toor first find the interaction energy of a chain with a lateral field with a neighboring chain. To first order in the deformation, the transverse fluctuations perpendicular to the plane defined by the chains do not contribute to the interaction energy. More importantly, the interaction has a strong peak at $k\rho \simeq 1$, which indicates that only fluctuation modes with wavelength on the order of the separation distance will interact strongly. The deformation energy due to the fluctuation mode depends on ϵ_l and ϵ_t, the longitudinal and transverse stiffness energies, which scale as $m^2/\mu_0 a^3$.

The total energy contributes to the partition function resulting in the free energy for the chains,

$$F(\rho) = -176 \frac{k_B T}{2\pi} \frac{L a^4}{\rho^5}, \tag{5}$$

as a power-law decay. It is important to note that the calculated interaction is independent of the applied field strength. Although higher field strengths increase the interaction energy, the effect is canceled by a suppression of the fluctuations as the chains stiffen. In fact, this can be derived by assuming an acoustic spectrum for the phonon modes, noting that equipartition gives $\langle |u(k)|^2 \rangle = k_B T/\epsilon k^2$, where ϵ is again an elastic energy for the fluctuation mode, $\epsilon \sim m^2/\mu_0 a^3$. Halsey and Toor show that the mean-squared field around a fluctuating chain scales as

$$\langle H^2 \rangle \sim \frac{m^2 k_B T}{\mu_0^2 \rho^4 a^2 \epsilon} \sim \frac{k_B T a}{\mu_0 \rho^4}. \tag{6}$$

Unlike the rigid dipolar chains, the root mean-square lateral field for fluctuating chains decays as a power law and is independent of field strength.

C. Modified Halsey-Toor model

The independence of lateral interactions of the field strength predicted by the HT model has motivated several studies of chain dynamics and structural formation in MR and ER suspensions [9,12,16,17]. In their study of ER suspension coarsening, Martin and co-workers observe a power-law dependence of the suspension coarsening with the applied field strength in disagreement with the HT model [9,12]. They proposed an extension of the HT model that accounts for this dependence on field strength, although the basic premise of the modified Halsey-Toor (MHT) theory is the same—thermal fluctuations of chains induce interactions that drive the lateral coalescence.

Martin *et al.* note that a chain with a dipole moment per unit length $m/a \sim \mu_0 \chi a^2 H$ interacts with the mean-squared lateral field induced by chain fluctuation. Using Eq. (6), the interaction energy per unit length a is on the order

$$U \sim (m/a)\langle H^2 \rangle^{1/2} \sim \frac{\chi H (\mu_0 k_B T)^{1/2} a^{5/2}}{\rho^2} \tag{7}$$

and can be either repulsive or attractive.

The time scale for chain coalescence is found by balancing the fluctuation force experienced by a chain segment ξ from Eq. (7) and the viscous drag on the segment. When the coalescence time scale τ_c is much shorter than the characteristic relaxation time of the fluctuations τ_f, the fluctuations persist long enough to drive the coarsening process. The mechanism is favored by the fact that fluctuations with long wavelengths $k \sim \rho$ dominate the lateral field [6]. However, the condition that $\tau_c \ll \tau_f$ is generally applicable only in moderately to highly concentrated suspensions where the initial chain separation will be small. For instance, Martin *et al.* investigated ER suspensions with volume fractions $\phi \sim 0.03$ [12].

Fermigier and Gast also observed the side-by-side coalescence of dipolar chains [4]. In their study, the two-dimensional aggregation kinetics of superparamagnetic latex particles were observed with microscopy. At sufficiently high particle surface fractions ($\phi_e \sim 0.03$), the suspension rapidly forms long, concentrated chains in the field direction. The interchain spacing is small, and the authors observed lateral chain coalescence through a ''zippering'' motion. The chains contact in one spot and the remainder of the chain on both sides of the contact zips together rapidly. These observations are consistent with MHT theory in which a large-amplitude fluctuation draws two chains together and initiates the aggregation before having enough time to relax. Unfortunately, the field dependence of this process was not studied.

D. Defect-driven interaction

Both the HT and MHT models show that the thermal fluctuations of dipolar chains create a long-range lateral field that increases the range of interaction driving the suspension coarsening. Likewise, chain defects also create local variations in the dipole moment density along a chain and break the symmetry of the lateral field. In another recent work, Martin *et al.* used computer simulations of dipolar suspension aggregation to show that coarsening can occur in the absence of thermal fluctuations [10].

This defect-driven coarsening is discussed for concentrated suspensions ($\phi \sim 0.05$–0.50), which have a greater tendency to form highly irregular chains. In their simulation visualizations, Martin *et al.* showed that single particles or groups of particles tend to cling to the sides of chains, which causes them to interact strongly in the absence of thermal fluctuations, driving them toward further coarsening. Similar defective structures were experimentally observed for MR suspensions [13].

E. Interactions and coarsening

As we discussed in the preceding sections, several physical processes account for the lateral interaction of chains, including the behavior of rigid chains, thermally induced interactions in the HT and MHT models, and defect-driven interactions. It is useful to consider under what conditions each of these processes will dominate the long-time coarsening of dipolar suspensions. We expect the strength of dipolar interactions and the volume fraction to play particularly important roles. The dipole strength influences the stiffness of chains, the thermal modes excited, and the potential for kinetic trapping of chain defects. As the volume fraction increases we move from dilute chains that form slowly and interact over long separations to systems where chains grow

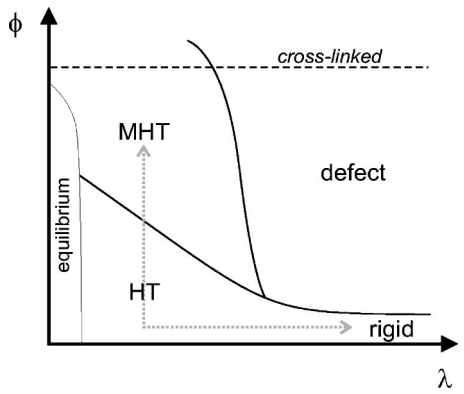

FIG. 2. Dominant mechanisms of lateral interactions with respect to regimes of dipolar interaction and initial volume fraction. The dashed, gray lines indicate regions where experiments were conducted.

rapidly and in close proximity. Figure 2 shows how one might partition these regimes of concentration and interaction strength to underlying interactions. This figure is meant to be illustrative and considers a system in which a dc field is applied instantaneously. In contrast, ramping the field may limit the formation of defects, since structures will not be kinetically pinned into defective chains as they begin to form.

At low concentration, the chains are dilute and well separated. In the limit of low field strengths ($\lambda \leqslant 5$), the chain length equilibrates and further suspension coarsening is suppressed [4]. At higher dipole strengths, long-range interactions between fluctuating modes will play the dominant mechanism in chain coalescence, and therefore the HT model will describe the coarsening. At very high dipole strengths and low concentrations, relatively uniform chains form. These chains are too rigid to interact significantly through fluctuations, and may not coarsen at all under certain conditions. For instance, Fraden *et al.* observed no lateral coarsening in an ER suspension confined to the solid-liquid interface, presumably because the volume fractions limit chains to long separations and the two-dimensional diffusion time diverges as the chains grow [18,4]. Instead, the authors observed linear aggregates partitioning the space into strips.

At higher concentration, the separation between chains decreases. As the fluctuation amplitude scales with ρ, the MHT model becomes applicable. In this regime, chains attract and coalesce before a fluctuation relaxes. As discussed above, this is consistent with observations of chain zippering mechanisms and may explain the field dependence of light scattering studies of suspension coarsening [12].

Lastly, as we move to high dipole strengths at moderate and high particle concentrations, defective chains form as the structure is effectively pinned into configurations determined by the aggregation kinetics with little or no ability for further rearrangement. The defect-dominated region will be highly influenced by particle roughness, which contributes to pinning, as well as size polydispersity and magnetic heterogeneity.

Again, we emphasize that Fig. 2 is meant to illustrate the dominant interactions that may drive coarsening, starting from an initially disordered suspension and applying an instantaneous, dc field. If we imagine bringing two fluctuating chains together from infinite separation, the interaction in the far field may be HT-like, while at closer separations, we may observe elements of rigid and MHT behavior. For instance, the gray, dashed lines in Fig. 2 illustrate the regions relevant to our optical trapping experiments. By starting with flexible chains at fairly long separations, we investigate the far-field fluctuation-mediated interactions between chains. Because the fluctuation relaxation time is much less than the aggregation time in this case, the dominant interaction should be governed by the HT model. By reducing the separation between chains, the aggregation time approaches the fluctuation relaxation. We expect, then, that the near-field behavior will be dominated by MHT-like behavior. If instead we increase the dipole strength to large values, the finite chains we examine should stiffen to the point where fluctuations are significantly damped, and the chains will behave as rigid chains.

III. EXPERIMENTAL METHODS

Systems and techniques

To examine lateral interactions by direct microscopic manipulation, we use a ferrofluid emulsion synthesized following the fractionation method due to Bibette [19]. A mixture of ferrofluids (Ferrofluidics, EMG 905 and EMG 909), composed of monodomain Fe_3O_4 particles (100 Å) suspended in a hydrocarbon, is emulsified into water using sodium dodecyl sulfate, SDS (Sigma, cmc = 2.351 g/ml). The rough emulsion, consisting of particles between 0.1 and 10 μm in diameter, is fractionated through seven to nine successive depletion aggregations with SDS micelles. The particles are monodisperse and exhibit a superparamagnetic response to an applied field. We take advantage of this uniformity in particle shape, magnetic homogeneity, and size monodispersity to limit the contribution of defects in our experiments.

Our laser tweezers consist of two independently controlled traps generated by focusing an expanded beam from the 514.5 nm line of an Ar^+ laser (Lexel 95A) through a 63×NA1.2 water immersion microscope objective (Zeiss C-Apochromat). Force measurements on the order of 0.1 to 10 pN can be made by measuring the displacement of a particle from the trap center. The traps are calibrated for each experiment by measuring the displacement of a plain 3.5 μm polystyrene (PS) bead held far from surrounding interfaces ($\gtrsim 50$ μm) while the sample stage is translated at known velocities U in a medium with viscosity η, thus imparting a drag force of $6\pi a \eta U$. The displacement of the bead is analyzed by finding the center of mass of a thresholded image, with a position sensitivity better than 30 nm. The trap stiffness and maximum trapping force can be varied. Typical maximum trapping forces range between 3 and 12 pN.

Strong radiation pressure from scattering and absorption due to the presence of iron oxide grains in the MR particles prevents us from trapping them. We apply the same ''tether-handle'' approach to manipulating chains described for our micromechanical experiments in Ref. [13]. Plain, streptavidin-coated polystyrene spheres are physically incorporated into the chain using an attached biotinylated magnetic bead. The PS spheres act as ''tethers'' with which we can manipulate the dipolar chains.

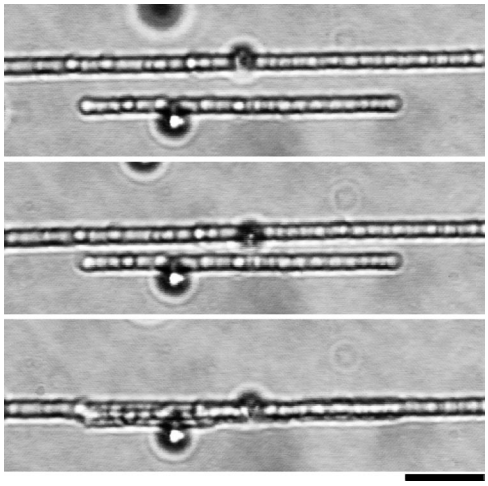

FIG. 3. Two chains exhibiting lateral attraction and subsequent coalescence. The bottom chain is held stationary with an optical trap while the top chain is left free to translate. The scale bar is 10 μm.

Figure 3 shows a video image of two chains interacting. In most of the experiments described here, one chain is held stationary while the other is initially positioned within 10–12 particle diameters and released. The chains slowly approach until they coalesce. The trapped tether on the stationary chain allows us to measure the force experienced by the chain due to lateral interaction with the free chain. The force is determined by measuring the displacement of the tether in the trap. To minimize torque on the stationary chain, we select chains with the tether positioned close to the center. We can also measure the interaction between two chains at fixed separation by holding both chains with the laser traps. This is especially useful for measuring the interaction at fixed separations while the dipole strength is varied.

In order to interpret the lateral interactions between chains, we characterize their mechanical stiffness and fluctuation dynamics using videomicroscopy. Samples are prepared identically with the exception that no tether handles are introduced. We form dilute chains up to 50 μm long in a dc field between 5100 and 6400 A/m ($\lambda = 610$–960). We observe the fluctuations of the dipolar chains microscopically as the interaction strength is varied between $\lambda = 150$ and 610 ($H = 2500$–5100).

Images of isolated fluctuating chains are captured to a video recorder and transferred to a computer in the form of image stacks. Individual frames are captured at 10 Hz. The chain center is found by stepping along each image pixel column and fitting a Gaussian to the central intensity peak. While more computationally expensive, the Gaussian fit provides excellent spatial resolution. It is known that center-finding routines that identify intensity maxima are able to locate centroids to within one-half a pixel [20]. For a Gaussian fit, the standard deviation of the position measurement is easily reduced to 1/10 pixel [21]. Typically, our position accuracy is ~ 0.12 pixel, corresponding to a spatial resolution of 15 nm. We show a sample image of a chain in Fig. 4. The central line marks the chain center found using image processing. This data representation of the chain is then analyzed to extract the amplitude and relaxation time of long-mode lateral fluctuations.

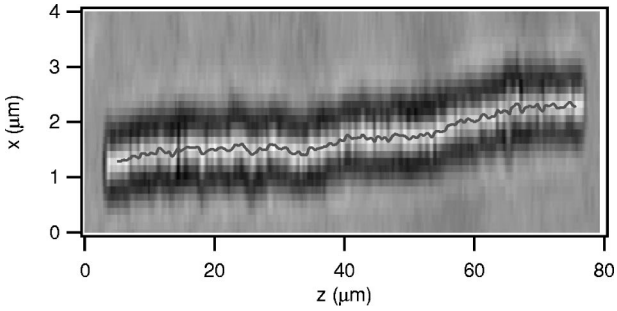

FIG. 4. Sample frame of fluctuating dipolar chain. The solid line traces the center of the chain found by our image processing algorithm. Note that the vertical axis has been magnified by a factor of 20.

IV. RESULTS AND DISCUSSION

A. Chain dynamics

In Fig. 5 we plot the root-mean-squared transverse displacement $\langle \delta^2(s) \rangle^{1/2}$ versus the separation between two points on the chain scaled by the particle diameter s/d at dipole strengths $\lambda = 150$,240, and 610. As expected, the magnitude of fluctuations decreases with increasing dipole strength, indicating the stiffening of the chains as the interaction between particles becomes stronger. At the highest field strength, $\lambda = 610$, the end-to-end deviation is on average less than one-tenth of a particle diameter.

The constrained motion of particles within dipolar chains should be similar to the dynamics of other colloidal aggregates, including the dynamics of fractal colloidal gels. In fact, here we show that the local-mode model developed by Krall and Weitz [22] to describe the internal dynamics of colloidal gels can be used to model the fluctuations of dipolar chains over a broad range of length and time scales. The similarity of behavior is not entirely surprising, since linear chains are essentially aggregates with a fractal dimension $d_f = 1$.

In an overdamped system such as dipolar chains or fractal aggregates, fluctuations are localized to a length s. The con-

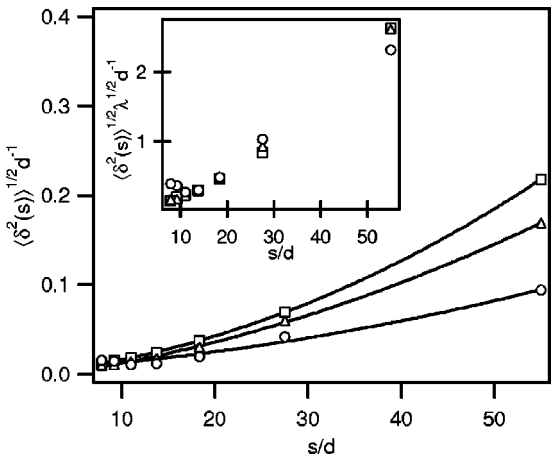

FIG. 5. Root-mean-squared amplitude of long-wavelength fluctuations versus fluctuation mode for a dipolar chain. The curves represent quadratic fits to the data, in agreement with the local-mode model. Scaling the δ with $\lambda^{1/2}$ collapses the data (inset). The scaling is consistent with HT and MHT theories.

tribution of a mode of length s to the mean-squared displacement of a chain segment ξ is

$$\langle \Delta r_\xi^2(t)\rangle = \frac{2k_BT}{n(s)\kappa(s)}[1-e^{-t/\tau(s)}]. \tag{8}$$

The relaxation time scale is determined by viscous relaxation $\tau(s)=6\pi\eta s/\kappa(s)$. The amplitude of the local fluctuation given by Eq. (8) is found by equipartition, noting that the energy localized within a region s is reduced by the number of regions of the same size, $n(s)=N(a/s)$, where N is the total number of particles in the chain. The length-dependent spring constant is $\kappa(s)=\kappa_0(a/s)^\beta$, where κ_0 is the effective spring constant between two particles in the chain and $\beta=2+d_b=3$ is the elasticity exponent as a function of the bond dimension [23,24]. As in fractal colloidal gels, this length dependence reflects the fact that pulling on the aggregate causes it to unbend rather than stretch [24]. We demonstrated this in our previous work by applying linear tensions to chains with optical traps and measuring the resultant small strain increases consistent with unbending [13,25].

We can estimate κ_0 by considering the energy required to displace a particle laterally by a distance δ from an otherwise straight chain. The point dipole interaction energy between two particles along the chain separated by n other particles may be written for small δ as

$$U_n=\frac{\lambda d^3k_BT}{2}\left[\frac{1}{(n^2d^2+\delta)^{3/2}}-\frac{3n^2d^2}{(n^2d^2+\delta)^{5/2}}\right], \tag{9}$$

where d is the particle diameter. From Eq. (9), the restoring force is $F_n(\delta)=-\partial U/\partial\delta$. Expanding this force around $\delta=0$ and keeping linear terms, we identify the spring constant κ_n,

$$F_n(\delta)=-\kappa_n\delta=\frac{-6\lambda k_BT}{d^2n^5}\delta. \tag{10}$$

To find κ_0, we take into account long-range interactions along the chain by summing κ_n over all neighboring particles,

$$\kappa_0=2\sum_{n=1}^{\infty}\frac{6\lambda k_BT}{d^2n^5}=\frac{12\zeta(5)\lambda k_BT}{d^2}, \tag{11}$$

where the zeta function is $\zeta(5)=\Sigma_{n=1}^{\infty}(1/n^5)\approx 1.037$.

Substituting our expressions for the spring constant $\kappa(s)$ and the number of modes $n(s)$ into Eq. (8), we expect fluctuation amplitudes to scale as s^2,

$$\frac{\delta(s)}{d}=\left(\frac{8}{3\zeta(5)N\lambda}\right)^{1/2}\left(\frac{s}{d}\right)^2. \tag{12}$$

Quadratic fits to the data in Fig. 5 show that the observed fluctuations are consistent with this scaling. The local-mode model also predicts that the amplitude will scale with interaction energy as $\delta\sim\lambda^{-1/2}$. By multiplying the measured amplitudes by $\lambda^{1/2}$ we collapse the data and verify this relation.

We can extend our analysis of chain dynamics to a broad range of time and length scales by applying the local-mode model to the dynamics probed using light scattering techniques. In a previous paper [26], we presented chain dynamics in terms of the mean-squared displacement $\langle \Delta r_\xi^2(t)\rangle$ with time measured using diffusing wave spectroscopy (DWS). DWS probes chain motion on timescales from 1 μs to 1 ms.

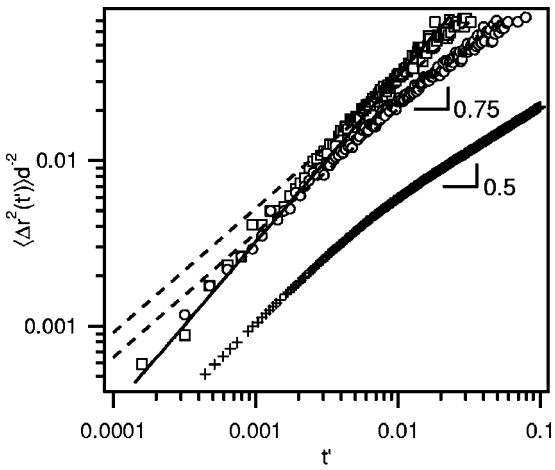

FIG. 6. Root-mean-squared displacement versus dimensionless time $t'=tD_sd^2$ for dipolar chains at field strength $\lambda=4$ (open squares) and $\lambda=16$ (open circles) using DWS results from Ref. [26] compared to the local-mode model of Krall and Weitz [22] (dashed lines). At short times, the chains exhibit a crossover from diffusive (solid line) to subdiffusive motion. The subdiffusive regime scales as $t^{0.75}$, unlike simulations (crosses), which exhibit Rouse-like behavior.

To find the motion of a chain segment due to the local dynamical modes, we integrate over fluctuations of all lengths weighted by the density of modes $-dn(s)/ds$ to find the mean-squared displacement with time. Nondimensionalizing length with respect to the particle diameter d and time with respect to the characteristic diffusion time for a particle $t'=tD_0d^{-2}$ yields

$$\langle \Delta r_\xi^2(t')\rangle d^{-2} = \frac{1}{6\zeta(5)\lambda}\int_0^N ds's'^2\{1-\exp[-12\zeta(5)\lambda s'^{-4}t']\}, \tag{13}$$

which can be written in terms of complete and incomplete gamma functions,

$$\langle \Delta r_\xi^2(t')\rangle d^{-2}=\frac{4N^3-[12\zeta(5)\lambda t']^{3/4}}{12}\left[3\Gamma\left(-\frac{3}{4}\right)+4\Gamma\left(\frac{1}{4}\right)-3\Gamma\left(-\frac{3}{4},\frac{12\zeta(5)\lambda t'}{N^4}\right)\right] \tag{14}$$

where $\Gamma(z)=\int_0^\infty t^{z-1}e^{-t}dt$ and $\Gamma(z,a)=\int_a^\infty t^{z-1}e^{-t}dt$. At short times, Eq. (14) scales as $t^{0.75}$. In Fig. 6 we compare the mean-squared displacement measured using DWS to the local-mode result.

The subdiffusive behavior is captured by the local-mode model with excellent quantitative agreement, especially since it should be noted that there are no adjustable parameters.

The mean-squared displacement scales as $\langle \Delta r_{\xi}^2(t) \rangle \sim t^{0.75}$ for all but the shortest times, in agreement with the model. For $\lambda = 16$, we find $\langle \Delta r_{\xi}^2(t) \rangle \sim t^{0.75}$ over two decades. At the earliest times, the DWS experiment captures the crossover from diffusive to subdiffusive motion, which is not described by the local-mode model. The crossover time decreases with increasing chain stiffness.

The $t^{0.75}$ scaling is identical to the dynamics of transverse fluctuations of semiflexible polymer molecules, such as actin [27,28], and is characteristic of the dynamics of an incompressible linear system with finite bending energy. We would therefore not expect the dynamics of dipolar chains to be described by the Rouse or Zimm models for flexible polymer molecules, which predict $\langle \Delta r_{\xi}^2(t) \rangle \sim t^{0.5}$ and $t^{0.67}$ scaling, respectively [29]. It is interesting to note that the Brownian dynamics simulations reported in [26] also demonstrate the diffusive to subdiffusive crossover; however, in the simulations the subdiffusive mean-squared displacement scales as $t^{0.5}$, as demonstrated in Fig. 6. Thus, the simulations predict behavior identical to the Rouse model, and in disagreement with the local-mode model. Granek has shown that hydrodynamic interactions in linear systems make only a marginal contribution to the relaxation [27]; therefore, it is more likely that the neglect of dipolar interactions beyond the nearest neighbors along the chain in the Rouse model and simulations is responsible for the disagreement at long times.

Combining DWS and videomicroscopy, we probe dynamics on time scales over six decades. For all but the shortest time scales, the local-mode model agrees with the observed dynamics. The local-mode model shows that the fluctuations of dipolar chains are consistent with the stiffness of a chain scaling with λ, or equivalently H^2. This is particularly important result for the HT theory, since the increase in stiffness, and subsequent decrease in fluctuations, exactly cancels the increase in the dipolar interaction. As discussed in Sec. II, the theoretical result is a fluctuating lateral field and lateral interaction that is independent of the applied field.

B. Measured interactions

Direct measurements of lateral interactions are influenced by the length of the chains, relative orientation, and dipole strength. It is important to distinguish far-field and near-field behavior as well. As we discussed above in Sec. II, rigid chains interact weakly in the far field. As the chain flexibility increases, the far-field interaction will favor coupling between fluctuating modes, as described in the HT model. At these separations, the fluctuations relax before they can contribute significantly to a MHT-like interaction. As the separation is decreased to the near field, the relaxation of fluctuations plays a more significant role. Eventually, chains exhibiting sufficiently strong fluctuations will interact before the mode can relax, similar to the zippering mechanism observed by Fermigier and Gast [4]. If the chains are constrained and stiff, the interaction will reflect the increased rigidity. Here we attempt to understand the measured lateral interactions between dipolar chains in this context, taking into account their fluctuation behavior. We discuss three cases that highlight the diverse behavior: in the first case, we observe a long-range, purely attractive interaction between flexible chains, as predicted by the HT model. In the second case, we measure the interaction between two short, rigid chains and show that the interaction is repulsive in the far field and attractive only at much closer separations than for fluctuating chains. Finally, in the third case we demonstrate that the near-field behavior of fluctuating chains is not necessarily purely attractive, but can exhibit strong and sudden changes between attraction and repulsion. We follow this by showing that these deviations increase in intensity and duration as the field strength increases.

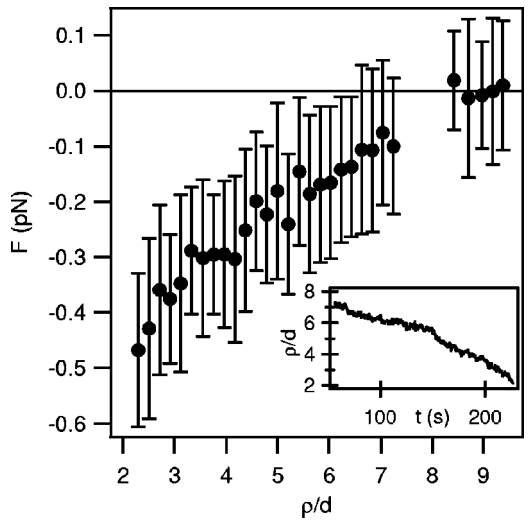

FIG. 7. Lateral force between fluctuating dipolar chains and corresponding chain separation with respect to time (inset) for $\lambda = 340$. The chains exhibit a long-range attractive interaction. An image of the chains is shown in Fig. 3.

In the first case, two chains laterally attract at $\lambda = 340$ and coalesce, as shown in Fig. 3. The bottom chain is held stationary while the top chain is initially held, positioned, then released. The inset in Fig. 7 shows the average chain separation versus time as the free chain slowly moves toward the stationary chain. As the chain separation decreases, we measure an increasingly strong lateral attraction by the displacement of the stationary tether. When the force is plotted versus the chain separation in Fig. 7, it becomes apparent that a long-range attractive interaction, starting at a separation $\rho \approx 8d$, draws the chains together. The maximum measured attraction averages 0.5 ± 0.2 pN.

Figures 8 and 9 show a similar experiment conducted at $\lambda = 610$ where we see startlingly different behavior. The chains are short and rigid; by videomicroscopy, the longest fluctuation mode has an amplitude $\delta \sim 0.05d$. As shown in the inset of Fig. 9, the chains repel one another when they are initially held at a separation $\rho = 4.8$ μm and one is released. We reposition the chains closer and again they push apart. Only when the chains are separated by $\lesssim 4d$ do they

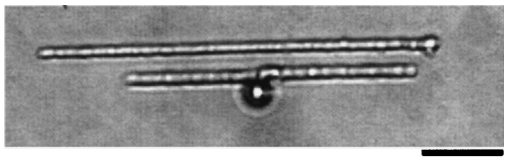

FIG. 8. Two short chains at $\lambda = 610$. The corresponding force profile is shown in Fig. 9. The scale bar is 10 μm.

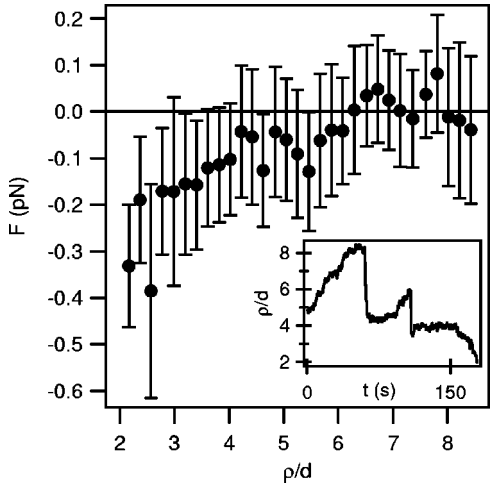

FIG. 9. Measured lateral force with respect to separation of two short chains at $\lambda = 610$. The inset shows lateral separation with respect to time. The chains exhibit far-field repulsion due to their stiffness and aligned ends that move them apart at separations $\rho \gtrsim 3d$. An image of the chains is shown in Fig. 8.

attract one another. The force profile measured during the experiment is shown in Fig. 9. Unlike the previous case, we do not observe a long-range lateral interaction between the chains. Instead, the behavior of the chains closely resembles the calculated interaction for two aligned, rigid chains discussed in Sec. II A and depicted in Fig. 1. Both the calculations and experiments exhibit a far-field repulsion and near-field attraction, and the range of these interactions is much less than those for flexible chains.

Stepping down the interaction strength, a measurement of two long chains at $\lambda = 240$ is shown in Figs. 10 and 11. Like the first case, the interaction begins at a long range and draws the chains together. The separation with time and the variation of force with separation are shown in Fig. 11. The initial interaction appears on the same length scale as our measurement at $\lambda = 340$, approximately $\rho \sim 8d$. However, the attraction grows much more quickly than in the previous case. As ρ decreases, a sudden shift from attractive to repulsive behavior is observed for $\rho \approx (4-5)d$, then a shift back. At the same time, the rate of decrease in the separation goes to zero and then reverses slightly. After about 15 s, the force becomes attractive again until the chains coalesce.

The sudden shift from an attractive to repulsive interaction at short separation resembles the behavior one would expect from the MHT model. Quick changes in sign indicate that the interactions between dipolar segments of one chain and the fluctuating field of another play a larger role in the near field. The interaction is enhanced by the larger amplitude of fluctuations due to the chain length and flexibility at

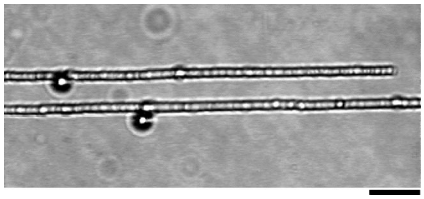

FIG. 10. Two chains at $\lambda = 240$. The corresponding force profile is shown in Fig. 11. The scale bar is 10 μm.

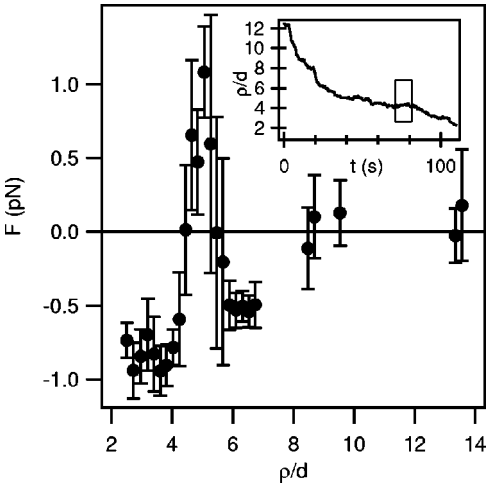

FIG. 11. Measured lateral force with respect to separation of two short chains at $\lambda = 240$. The inset shows lateral separation with respect to time. We observe a sudden switch to a repulsive interaction in the near field that resembles the MHT interaction. The boxed region in the inset highlights the point at which the chains begin to move apart, corresponding to the observed repulsion. An image of the chains is shown in Fig. 10.

$\lambda = 240$. The separation and force are consistent with observations put forth by Promislow [30], where chains fluctuated close to one another for several minutes before finally making contact and zippering together.

To further investigate the sudden instances of attraction and repulsion at short separations, we perform an experiment where both chains are held by optical traps at a close separation (approximately $\rho = 3.2d$) while the interaction strength is changed from $\lambda = 340$ to 610. The chains are limited to a range of motion around the fixed position, determined by the stiffness of the laser trap. This prevents coalescence induced by a fluctuation for all but the strongest displacements. Figure 12 shows the force measured with respect to separation of the chains. At $\lambda = 340$, the force is on average attractive at 0.2 pN, but deviates for brief periods

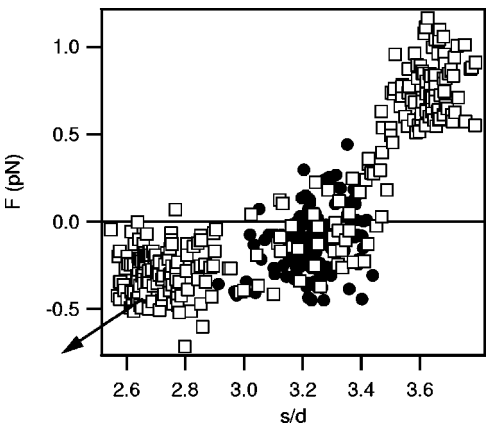

FIG. 12. The near-field behavior of two dipolar chains at fixed separation, where both chains are held by optical traps. At $\lambda = 340$ (circles) we observe attractive and repulsive interactions that cause the chains to move together or apart, respectively. At $\lambda = 610$ (squares), the interaction and deviations increase substantially, resulting in coalescence, as indicated by the arrow.

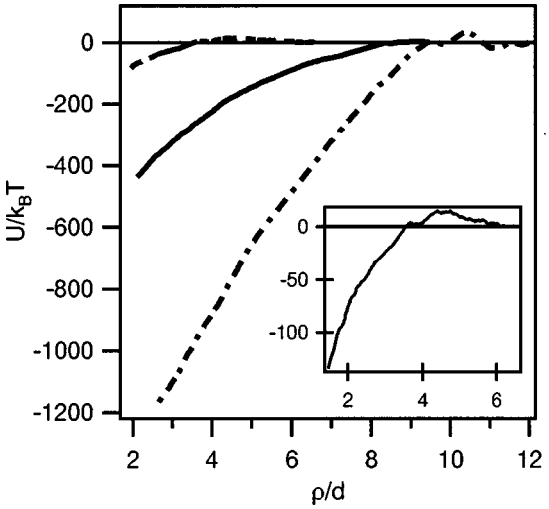

FIG. 13. Average attractive lateral interaction potential for $\lambda = 240$, 340, and 610. The $\lambda = 610$ case is expanded in the inset.

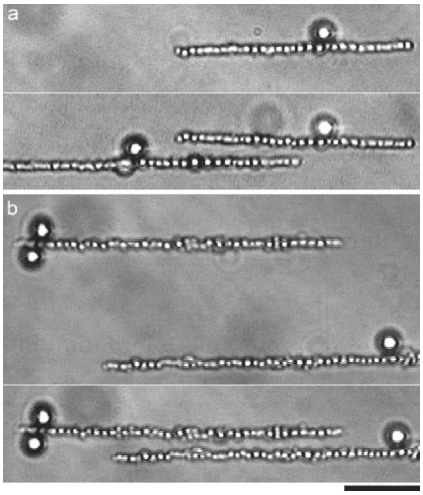

FIG. 14. The effects of defects on the lateral interaction. (a) A single size defect induces a repulsion between two laterally interacting chains. (b) Multiple defects induce a lateral attraction, causing two coarse chains to bend towards one another. The scale bar is 10 μm.

toward stronger attraction or repulsion. The attraction pulls the chains to closer separations, while the repulsion pushes them away. Deviations are on the order of $\rho \approx 0.2d$. As we increase the interaction to $\lambda = 610$, these deviations become stronger and last longer. Sudden shifts from attraction to repulsion are observed, forcing the separation to change by $\pm 0.5d$. During the last advance toward one another, the chains coalesce, as indicated by the arrow in Fig. 12. In this case, a fluctuation pushed the chains to a separation where the attractive force was stronger than the trap stiffness.

To summarize our findings, we integrate the force-separation profiles to find the interaction energies for the three cases described above, as shown in Fig. 13. In the $\lambda = 240$ case, the repulsion was subtracted to find the average attractive interaction. For flexible chains, a long-range interaction is evident, consistent with the HT theory. There are two dominant field dependencies: the first, illustrated by the potentials in Fig. 13, is due to the stiffening of finite chains. As the rigidity of the chains increases, the interaction becomes short ranged with a repulsive barrier. The second observed field dependence is in the near field. As described above for two chains held at close separation, higher field strengths cause stronger interactions, both attractive and repulsive, consistent with the MHT model. From these experiments we see that the interaction of finite chains is complex—the length of the chains can mediate the stiffness and the amount that the ends interact. The interaction also depends on whether the chains are in the far or near field. As such, no single mechanism or model in the literature describes all regimes of lateral chain interaction and suspension coarsening.

It is important to note that we use monodisperse, magnetically homogeneous particles, supporting the idea that thermal fluctuations, and not chain defects alone, can be responsible for suspension coarsening. Since defects can cause significant distortions in the lateral field, we will conclude by showing two cases where defects alter the lateral interaction. In Fig. 14(a) the end of the top chain interacts strongly with a large particle on the otherwise uniform lower chain when they are brought together, causing the chains to deflect from one another. In Fig. 14(b) two coarse chains are brought into proximity. While the deflection is less dramatic than in the previous case, the chains do bend toward one another by as much as $0.5d$, indicating an attractive lateral interaction.

V. CONCLUSIONS

In this paper, we presented observations on the direct measurement of lateral interactions between dipolar chains using optical trapping. Lateral interactions govern the long-time evolution of suspension structure. Several theories describe the lateral interaction of chains. Rigid chains are expected to interact only at short separations, while the HT and MHT theories show that fluctuation-fluctuation and fluctuation-dipole coupling cause chains to exhibit a long-range lateral interaction. The dominant mechanism for chain coalescence depends on several factors, including the concentration regime, the strength of the dipolar interaction, and the tendency of the system to form defects due to the aggregation kinetics, particle polydispersity, roughness, or magnetic heterogeneity.

In fact, our direct measurements of the lateral interactions confirmed this rich variety of behavior. We found that flexible chains exhibit a long-range attraction in agreement with the HT model. However, we observed two major field dependencies: a transition to rigid-chain behavior as the dipole strength is increased for short chains, consistent with the stiffness measured by videomicroscopy, and sudden switches between repulsion and attraction at close separations before final coalescence. These sudden sign changes, which increase in intensity with field strength, are consistent with the near-field behavior of the MHT model.

Videomicroscopy and light scattering measurements of the transverse fluctuations of the chains are in good agreement with a local-mode analysis of the dynamics. We find the the chain stiffness increases with H in agreement with the HT and MHT models. It is interesting to note that the mean-squared displacement crosses over from diffusive to subdiffusive motion which scales as $t^{0.75}$, as in semiflexible poly-

mers. A detailed understanding of this analogous behavior remains to be understood.

The structure, dynamics, and interactions of MR suspensions are interesting from a fundamental physical point of view. Dipolar interactions occur throughout nature, and because of their anisotropy and long range, can give rise to highly interesting and subtle effects, such as long-range lateral interactions between magnetic chains. Of particular interest is the dynamical similarities of dipolar chains to fractal colloidal gels and semiflexible polymers.

ACKNOWLEDGMENTS

The authors would like to thank M. Fermigier, L. LeGoff and F. Amblard for fruitful discussions. Support by NASA (Grant No. NAG3-1887-1) is gratefully acknowledged.

[1] W. B. Russel, D. A. Saville, and W. R. Schowalter, *Colloidal Dispersions* (Cambridge University Press, New York, 1989).
[2] M. Jolly, J.W. Bender, and J.D. Carlson, J. Intell. Mater. Syst. Struct. **10**, 5 (1999).
[3] S.J. Dyke, B.F. Spencer, Jr., M.K. Sain, and J.D. Carlson, Smart Mater. Struct. **7**, 693 (1998).
[4] M. Fermigier and A.P. Gast, J. Colloid Interface Sci. **154**, 522 (1992).
[5] D. Wirtz and M. Fermigier, Phys. Rev. Lett. **72**, 2294 (1994).
[6] T.C. Halsey and W. Toor, J. Stat. Phys. **61**, 1257 (1990).
[7] T.C. Halsey and W. Toor, Phys. Rev. Lett. **65**, 2820 (1990).
[8] W. Toor, J. Colloid Interface Sci. **156**, 335 (1993).
[9] J.E. Martin, J. Odinek, and T.C. Halsey, Phys. Rev. Lett. **69**, 1524 (1992).
[10] J.E. Martin, K.M. Hill, and C.P. Tigges, Phys. Rev. E **59**, 5676 (1999).
[11] J. Liu *et al.*, Phys. Rev. Lett. **74**, 2828 (1995).
[12] J.E. Martin, J. Odinek, T.C. Halsey, and R. Kamien, Phys. Rev. E **57**, 756 (1998).
[13] E.M. Furst and A.P. Gast, Phys. Rev. E **61**, 6732 (2000).
[14] E. M. Lifshitz and L. P. Pitaevskii, *Statistical Physics*, 2nd ed. (Pergamon, Oxford, 1980).
[15] J. M. Israelachvili, *Intermolecular and Surface Forces*, 2nd ed. (Academic Press, San Diego, 1992).
[16] A. Silva, B. Bond, F. Plouraboué, and D. Wirtz, Phys. Rev. E **54**, 5502 (1996).
[17] M. Hagenbüchle and J. Liu, Appl. Opt. **36**, 7664 (1997).
[18] S. Fraden, A.J. Hurd, and R.B. Meyer, Phys. Rev. Lett. **63**, 2373 (1989).
[19] J. Bibette, J. Colloid Interface Sci. **147**, 474 (1991).
[20] W. Schaertl and H. Sillescu, J. Colloid Interface Sci. **155**, 313 (1993).
[21] J.C. Crocker and D.G. Grier, J. Colloid Interface Sci. **179**, 298 (1996).
[22] A.H. Krall and D.A. Weitz, Phys. Rev. Lett. **80**, 778 (1998).
[23] P. Meakin, Phys. Rev. Lett. **51**, 1119 (1983).
[24] Y. Kantor and I. Webman, Phys. Rev. Lett. **52**, 1891 (1984).
[25] E.M. Furst and A.P. Gast, Phys. Rev. Lett. **82**, 4130 (1999).
[26] E.M. Furst and A.P. Gast, Phys. Rev. E **58**, 3372 (1998).
[27] R. Granek, J. Phys. II **5**, 1349 (1995).
[28] F. Amblard *et al.*, Phys. Rev. Lett. **77**, 4470 (1996).
[29] M. Doi and S.F. Edwards, *The Theory of Polymer Dynamics* (Clarendon, New York, 1986).
[30] J. H. E. Promislow, Ph.D. thesis, Stanford University, 1997.